東北大学機関リポジトリ
TOUR
Tohoku University Repository

Determination of order parameter of L10-FePd nanoparticles by electron diffraction

著者	Sato Kazuhisa, Hirotsu Yoshihiko, Mori Hirotaro, Wang Zhouguang, Hirayama Tsukasa
journal or publication title	Journal of Applied Physics
volume	97
number	8
page range	084301
year	2005
URL	http://hdl.handle.net/10097/52206

doi: 10.1063/1.1861987

HTML ABSTRACT + LINKS

Determination of order parameter of $L1_0$–FePd nanoparticles by electron diffraction

Kazuhisa Sato[a] and Yoshihiko Hirotsu
The Institute of Scientific and Industrial Research, Osaka University, 8-1 Mihogaoka, Ibaraki, 567-0047, Japan

Hirotaro Mori
Research Center for Ultra-High Voltage Electron Microscopy, Osaka University, Yamadaoka, Suita, 565–0871, Japan

Zhouguang Wang and Tsukasa Hirayama
Japan Fine Ceramics Center (JFCC), 2–4–1 Mutsuno, Atsuta-ku, Nagoya, 456-8587, Japan

(Received 19 July 2004; accepted 22 December 2004; published online 31 March 2005)

Long-range order (LRO) parameters of two-dimensional dispersed single-crystalline 10-nm-sized FePd nanoparticles with the $L1_0$ structure have been determined accurately by electron diffraction in transmission electron microscopes (TEMs) under accelerating voltages of 300 kV and 1 kV. Diffraction patterns by exciting *hh*0 systematic reflections effectively reduced the numbers of diffracted beams and simplified the thickness dependence of intensity ratio I_{110}/I_{220} for 110 and 220 reflections. Mean thickness of the nanoparticles was estimated to be 7.8 nm by electron holography. The relation between the intensity ratio and the order parameter was calculated on the basis of multiple-scattering intensity calculation. By comparing the relation and experimentally obtained intensity ratios, the order parameters of 0.65 and 0.79 were obtained using 300-kV TEM for FePd nanoparticles after annealing at 873 K for 3.6 and 36 ks, respectively. Also, the order parameter of 0.82 was obtained using 1-MV TEM for the same specimen annealed at 873 K for 36 ks. These order parameters were determined using the Debye–Waller factors for bulk Fe and Pd. The order parameter decreased about 7.3% when a very large Debye–Waller factor as large as 0.01 nm^2 was assumed. A combination of electron diffraction under the conditions of *hh*0 systematic reflections and the diffraction experiment at the high accelerating voltage makes the LRO parameter analysis easy and correct. © *2005 American Institute of Physics*.
[DOI: 10.1063/1.1861987]

I. INTRODUCTION

Recent development of high-density magnetic recording media results in a rapid increase of its recording density, which, however, is reaching nearly the maximum value for the conventional longitudinal recording media.[1–5] For future ultrahigh density magnetic recording media, one of the candidates is the high-density assembly of two-dimensional distributed isolated hard magnetic nanoparticles with sizes smaller than 10 nm in an insulating film, aiming at the increase of storage density and the decrease of recording noise. $L1_0$-type (CuAu I-type) FePt-, CoPt-, and FePd-ordered alloy nanoparticles have attracted much interest for future ultrahigh density magnetic storage media because of their high thermal stability due to the larger magnetocrystalline anisotropy constant (K_u), as well as the larger saturation magnetization compared to those of today's recording media composed of CoPtCr-based alloys.[5] Since the large K_u values of $L1_0$–FePt or FePd alloys are originated from their tetragonal ordered structures, it is necessary to evaluate the degree of atomic order of those structures when the hard magnetic properties are discussed. For hard magnetic FePt thin continuous films, several reports have been presented on the long-range order (LRO) parameters (S),[6,7] where S values were determined by using the integrated intensities obtained from x-ray diffraction based on the kinematical scattering theory.[8] Very recently, a relation of a gradual increase of K_u with S has been reported[9,10] by two research groups for $L1_0$-FePt films. However, for small isolated $L1_0$ nanoparticles, detailed studies of S and the K_u relation have not been performed so far. The following is thought to be the main reasons especially for the absence of systematic reports on the S values as a function of particle size: A small volume fraction of $L1_0$ nanoparticles in the specimen volume results in a small signal-to-noise (S/N) ratio for the $L1_0$ structure in x-ray diffraction profiles in addition to the broadening of diffraction peaks due to the smallness of the particles. To overcome the experimental difficulty and to determine the LRO parameter of very small $L1_0$ nanoparticles precisely, electron diffraction has a great advantage in obtaining the superlattice and fundamental reflections from the small volume of $L1_0$ nanoparticles,[11] primarily because the scattering amplitude of atoms for electrons is much larger than that for x rays.[12] However, in electron-diffraction intensity analysis, multiple scattering becomes inevitable due to the strong electron scattering. The multislice approach is known as a useful method for calculating the intensity of electrons propagating through crystals.[13] Transmitted and diffracted beam intensi-

[a]Electronic mail: sato@sanken.osaka-u.ac.jp

 © 2005 American Institute of Physics

Downloaded 26 Aug 2011 to 130.34.134.250. Redistribution subject to AIP license or copyright; see http://jap.aip.org/about/rights_and_permissions

ties after the multiple scattering (dynamical scattering) can be evaluated precisely by the multislice calculation when such experimental parameters as specimen thickness, incident-beam direction, specimen composition, lattice parameter, and temperature factor (Debye–Waller factor: B) are known in addition to the crystal structure. In order to evaluate the order parameter precisely by a conventional selected area electron diffraction (SAED), several conditions are required for specimens. Primarily, a preferential texture for which the intensity analysis becomes complicated should be avoided. Randomly oriented, very small $L1_0$ nanoparticles with three-dimensional or two-dimensional distribution, or fully oriented, very small single-crystalline $L1_0$ nanoparticles with a two-dimensional dispersion are suitable for simplifying the intensity analysis. For the former case, very small $L1_0$ nanoparticles with random orientation make the kinematical scattering theory applicable for the diffraction intensity analysis as in the case of powder x-ray diffraction.[14] For the latter case, it is convenient to compare the diffracted beam intensity with the simulated ones because of the simple scattering geometry. In this study the authors adopted the latter case. Here, well-isolated as well as two-dimensional dispersed nanoparticles on a flat substrate surface are necessary in order to avoid the multiple scattering of electrons among the nanoparticles. Also it is necessary to remove the nanoparticles film from the single-crystal substrate for electron-diffraction structure analysis in order to avoid the multiple scattering between the nanoparticles and the substrate. Furthermore, a covering layer on these nanoparticles is necessary for protecting the particles from oxidation. We selected a noncrystalline Al_2O_3 thin film as a cover layer to avoid multiple scattering of electrons between the nanoparticles and a cover layer.

Sato and Hirotsu have fabricated isolated single-crystalline $L1_0$–FePd nanoparticles epitaxially grown on NaCl substrate, where FePd nanoparticles are two-dimensionally dispersed and covered by an amorphous (a-) Al_2O_3 film to protect the nanoparticles from oxidation.[15] In transmission electron microscope (TEM) structural study, the nanoparticle film was removed from the NaCl substrate in distilled water. The above FePd nanoparticles satisfy the required experimental conditions mentioned above and suitable for the determination of the LRO parameter by electron diffraction. Magnetic hardening of these FePd nanoparticles due to the $L1_0$ phase formation has been reported in our previous article,[15] where a relatively smaller K_u than that of bulk alloys was derived. A precise determination of the LRO parameter for these particles is necessary for further quantitative discussion on the relation between the hard magnetism and the $L1_0$ ordering.

In this paper, we present a study of the LRO parameter of 10-nm-sized $L1_0$–FePd nanoparticles determined by electron diffraction operated at 300 kV and 1 MV by taking the dynamical scattering of electrons into consideration. The advantages of using systematic reflections and high-voltage electron diffraction in determining the LRO parameter are also discussed. Also discussed are the effects of the temperature factor and particles thickness on the LRO parameter of FePd nanoparticles.

II. EXPERIMENT

A. Specimen fabrication and characterization

FePd nanoparticles were fabricated by successive deposition of Pd and Fe onto cleaved NaCl substrates heated at 673 K, followed by a postdeposition annealing at 873 K. Evaporation was performed using an electron-beam evaporation apparatus (operated at 4 kV) with a base pressure of approximately 3×10^{-7} Pa. Pure Pd(99.95%), Fe(99.97%), and Al_2O_3 (99.99%) crystals were used as evaporation sources. In the process, we took advantage of the overgrowth of Fe nanoparticles onto Pd "seed" nanoparticles, which were epitaxially grown on the substrate surface. The as-deposited specimen was composed of nanocomplex particles of bcc Fe and Pd. The orientation relationships are as follows: $[011]_{Pd}\|[011]_{NaCl}$, $(100)_{Pd}\|(100)_{NaCl}$, $[100]_{Fe}\|[100]_{Pd}$, and $(011)_{Fe}\|(010)_{Pd}$. After the deposition of Fe, we further deposited an amorphous Al_2O_3 film in order to protect the particles from oxidation and also to avoid the particles coalescence on annealing. Postdeposition annealing at 873 K lead to a formation of FePd-ordered nanoparticles with the $L1_0$ structure. Here, we prepared two specimens with different annealing times of 3.6 and 36 ks for the postdeposition annealing at 873 K. According to energy dispersive x-ray spectroscopy (EDS) attached to TEM, the mean composition of the present specimen was found to be Fe-58 at. %Pd. Details of fabrication procedure, structural, and magnetic properties of FePd nanoparticles are shown in our previous article.[15] We observed SAED patterns by using two different TEMs with different accelerating voltages. One is the conventional 300-kV TEM (JEM-3000F) and the other is a high-voltage electron microscope operated at 1 MV (Hitachi, H-3000). Particle height (thickness) was estimated by electron holography operated at 200 kV (Hitachi, HF-2000).

B. Evaluation of LRO parameter by electron diffraction

The definition of the LRO parameter is as follows:[8]

$$S=\frac{r_\alpha-x_A}{y_\beta}=\frac{r_\beta-x_B}{y_\alpha}, \tag{1}$$

where $r_\alpha(r_\beta)$, $x_A(x_B)$, and $y_\alpha(y_\beta)$ denote the fraction of α sites (β sites) occupied by the right atom, the atom fractions represent the averaged alloy composition ($x_A=0.42$), and the fractions of α sites (β sites), respectively. In the present electron-diffraction study, the ratio of the 110 superlattice and 220 fundamental reflections has been used to evaluate the S value of the $L1_0$–FePd nanoparticles, since $L1_0$–FePd nanoparticles with their c axes oriented normal to the film plane are larger in number than those with c axes oriented parallel to the film plane.[15] The intensity ratio I_{110}/I_{220} strongly depends on the film orientation in SAED. In taking SAED patterns, $hh0$ systematic reflections were excited and the patterns were recorded using imaging plates (IP) for later quantitative analysis of diffracted beam intensities under different exposure times ranging from 0.5 to 8 s. In the reading process of electron intensities recorded in IPs, we took the fading effect of IP into consideration.[16] In order to evaluate

Downloaded 26 Aug 2011 to 130.34.134.250. Redistribution subject to AIP license or copyright; see http://jap.aip.org/about/rights_and_permissions

TABLE I. Numerical parameters used for multi slice calculations.

Alloy composition	Fe-58 at. %Pd	
Lattice parameters	$a=0.383$ nm, $c=0.366$ nm	
Zone axis	[001], [$\bar{1}14$], [$\bar{1}16$], [$\bar{1}18$], [$\bar{1}$ 1 10], and [$\bar{1}$ 1 12]	
Debye–Waller factor	0.0035 nm^2 (Fe), 0.0045 nm^2 (Pd)	
Spatial frequency limit	30 nm^{-1}	
Accelerating voltage	300 kV	1 MV
Slice thickness	0.14 nm	0.28 nm
Absorption (imaginary potential)	10% of real potential	

the I_{hh0} diffraction intensities correctly, intensities were calculated based on the multislice method[13] using a computer software, "MAC TEMPAS." The $L1_0$ structure belongs to the space group of $P4/mmm$, which gives the following structure factors of reflection, $F_{hkl}=4(x_{Fe}f_{Fe}+x_{Pd}f_{Pd})$ for *hkl* unmixed (all even or all odd) and $F_{hkl}=2|f_{Fe}-f_{Pd}|$ for *hkl* mixed. Numerical parameters used in this calculation are listed in Table I. In the calculation, we limited the reflections up to a spatial frequency of 30 nm^{-1}. The lattice parameters used here were determined from SAED patterns using a Pt fine polycrystalline thin film mounted on a Cu grid as "standard" for the camera-length correction. The measured lattice parameters were $a=0.383\pm0.001$ and $c=0.366\pm0.001$ nm with the axial ratio c/a of 0.955 ± 0.003 for FePd nanoparticles after annealing at 873 K for 36 ks, which were almost the same as those after annealing at 873 K for 3.6 ks within an experimental error.[15] The accurate value of the temperature factor for 10-nm-sized FePd nanoparticles is not known, so we took $B=0.0035$ and 0.0045 nm^2 for Fe and Pd, respectively, after the values for bulk metals.[17,18]

III. RESULTS

A. Structure and morphology of the oriented $L1_0$–FePd nanoparticles

$L1_0$–FePd nanoparticles fabricated by using Pd seed particles are well isolated as shown in Fig. 1 even after the annealing at 873 K for 36 ks. These particles are dispersed "two-dimensionally" on the substrate surface. The SAED pattern attached in the inset indicates the epitaxial growth of FePd nanoparticles. The 110 and 001 superlattice reflections in the ⟨100⟩ SAED pattern are from the oriented nanoparticles[15] with their crystallographic *c* axes normal and parallel to the film plane, respectively. *In situ* TEM observation on annealing up to 873 K revealed that a negligible particle coalescence occurred on annealing, which can be attributed to the "anchoring effect" of Pd seed nanoparticles. So it is said that both alloying and atomic ordering reactions proceed within each nanoparticles. Mean particle sizes measured from TEM images are listed in Table II as a function of annealing conditions. The particle size is defined here as the arithmetical mean of the minor and the major axes of the ellipse, and the total counting number was 200 from the TEM micrographs. Structural details analyzed by high-resolution TEM are shown in our previous study.[15]

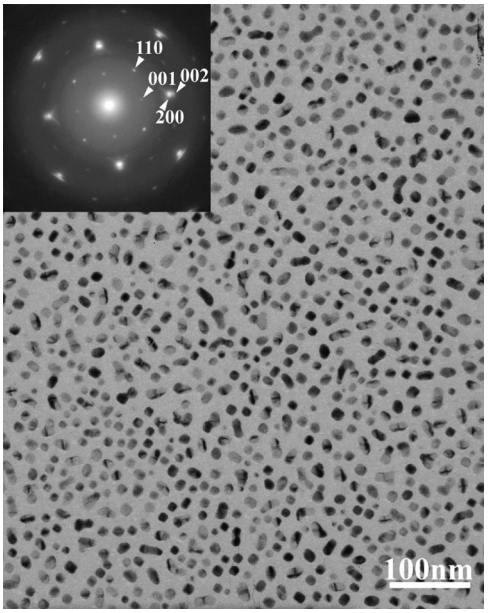

FIG. 1. A bright-field TEM image and the corresponding SAED pattern for $L1_0$–FePd nanoparticles after annealing at 873 K for 36 ks. Nanoparticles as small as 10 nm are uniformly dispersed. Epitaxial growth of FePd nanoparticles is clearly seen in the attached SAED pattern.

B. Estimation of the particle thickness by electron holography

In this study, the average particle thickness was estimated using electron holography. We can estimate the particle thickness using electron holography by taking advantage of the interference fringes formed by a transmitted wave from the nanoparticles and a reference wave. The fringe spacing Δt is written as[19,20]

$$\Delta t = \frac{2E\lambda}{V_0}, \tag{2}$$

where V_0 is the mean inner potential, λ the electron wavelength, and E the accelerating voltage. For λ and V_0 the relativistic corrections are made. The mean inner potential V_0 is written as

$$V_0 = V(000) = \left(\frac{h^2}{2\pi me}\right)\frac{1}{v_c}F(000), \tag{3}$$

where h represents the Planck's constant, m the mass of electron, e the electron charge, v_c the volume of the unit cell, and $F(000)$ the structure factor for the forward scattering for fast electrons ($\sin\theta/\lambda=0$, θ is the half of scattering angle, and λ the electron wavelength). Relativistic correction is performed for $F(000)$. A substitution of atom sites of Fe by Pd atoms due to the nonstoichiometric composition gives parameters

TABLE II. Mean particle size and deviation for FePd nanoparticles. Coalescence of particles on annealing is insignificant, indicating the result that both alloying and atomic ordering reactions occur in each nanoparticles.

	As-depro.	873 K–3.6 ks	873 K–36 ks
Mean size (D/nm)	11.3	11.1	11.3
Deviation ($\ln\sigma$)	0.23	0.18	0.21

Downloaded 26 Aug 2011 to 130.34.134.250. Redistribution subject to AIP license or copyright; see http://jap.aip.org/about/rights_and_permissions

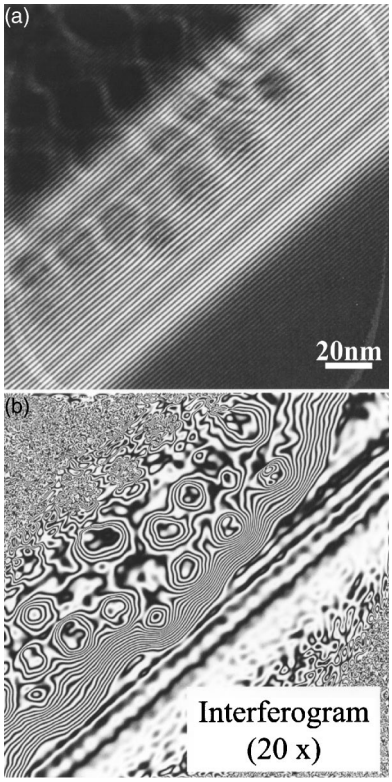

FIG. 2. (a) An electron hologram image for FePd nanoparticles. Fringes due to the interference are clearly seen. (b) An interferogram processed from Fig. 2(a) (amplification: $\times 20$). Fringes due to the phase changes are clearly seen within the nanoparticles.

r_α, r_β as $r_\alpha = 0.84$, and $r_\beta = 1$ for fully ordered $L1_0$–FePd ($S = 0.84$ for 58 at. %Pd). Here, the "right" atom on the α site was set to be Fe. Thus, the structure factor $F(000)$ is expressed as follows:

$$F(000) = 2(r_\alpha + w_\beta)(f_{\mathrm{Fe}} m/m_0) + 2(r_\beta + w_\alpha)(f_{\mathrm{Pd}} m/m_0),$$

$$= (4m/m_0)(x_{\mathrm{Fe}} f_{\mathrm{Fe}} + x_{\mathrm{Pd}} f_{\mathrm{Pd}}), \quad (4)$$

where $m/m_0 (=1.3914)$ is the relativistic electron mass ratio for electrons accelerated at 200 kV.[12] From Eqs. (3) and (4), V_0 is estimated to be 26.3 V for $L1_0$–FePd ($S = 0.84$) where the atomic scattering factors, f_{Fe} and f_{Pd}, at $\sin\theta/\lambda = 0$ were taken from the table calculated by Rez *et al.*[21] Figure 2 shows an electron hologram [Fig. 2(a)] and an interferogram [Fig. 2(b)] obtained by electron holography at 200 kV for FePd nanoparticles after annealing at 873 K for 3.6 ks. In Fig. 2(b), fringes are observed within the particles. These fringes are due to the phase shift produced by the crystal potential change with the change of crystal thickness. From the profiles of these fringes, it is found that all the FePd particles have flat surfaces parallel to the substrate plane, and are almost pyramidlike shape with curved corners and truncated flat top surfaces. Equation (2) gives a value of 38.1 nm/fringe for the present $L1_0$–FePd particles. By measuring the number of fringes for each particle in Fig. 2(b), we constructed a histogram of particle thickness distribution, as shown in Fig. 3. The mean particle thickness obtained was 7.8 nm with standard deviation of $\ln\sigma = 0.24$ (Log-normal-type distribution). The population of the particles with thickness thinner than 10 nm is about 90% in the histogram.

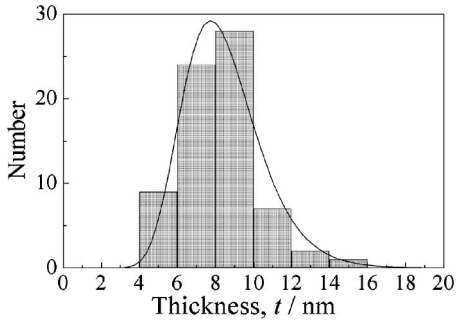

FIG. 3. Thickness distribution of FePd nanoparticles determined from electron holography shown in Fig. 2. The mean thickness was 7.8 nm with standard deviation ($\ln\sigma$) of 0.24.

C. Determination of the LRO parameter by electron diffraction at 300 kV

It was found that a slight beam tilting from the [001] incidence towards the $[\bar{1}10]$ direction results in an excitation of *hh*0 systematic reflections, which reduces diffracted beams and can largely decrease and simplify the multiple-scattering events among the transmitted and the diffracted waves. According to the multislice calculations, the intensity ratio I_{110}/I_{220} shows an oscillation with specimen thickness under the [001] incidence even from very thin regions below 15 nm thick, while in the case of $[\bar{1}14]$, $[\bar{1}16]$, $[\bar{1}18]$, $[\bar{1}1\ 10]$, or $[\bar{1}1\ 12]$ incidences, the intensity ratio increases monotonically with thickness, as shown in Fig. 4. In the following, we focus on the intensity analysis of SAED patterns with the beam incidence of $[\bar{1}16]$, where weak reflections other than the *hh*0 systematic reflections are also taken into consideration in the multislice calculation within the aperture limitation of 30 nm^{-1}. The beam tilting angle of about 0.23 rad for $[\bar{1}16]$ incidence resulted in a correction of the specimen thickness (t) based on the relation, $t/\cos\phi$, where ϕ denotes the tilting angle. As a result, the corrected thickness was 8.0 nm in the present experiment.

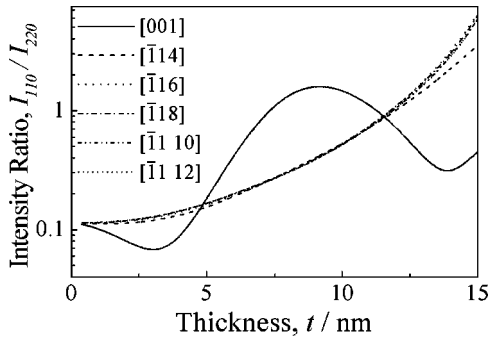

FIG. 4. Thickness dependence of the calculated intensity ratio, I_{110}/I_{220}, for several beam incidences under $S = 0.8$. The intensity ratio oscillates in the case of [001] incidence (net pattern) even in the thickness region below 15 nm, while the intensity ratios monotonically increase in the case of $[\bar{1}14]$, $[\bar{1}16]$, $[\bar{1}18]$, $[\bar{1}1\ 10]$, and $[\bar{1}1\ 12]$, where the *hh*0 systematic reflections are excited in the diffraction pattern.

Downloaded 26 Aug 2011 to 130.34.134.250. Redistribution subject to AIP license or copyright; see http://jap.aip.org/about/rights_and_permissions

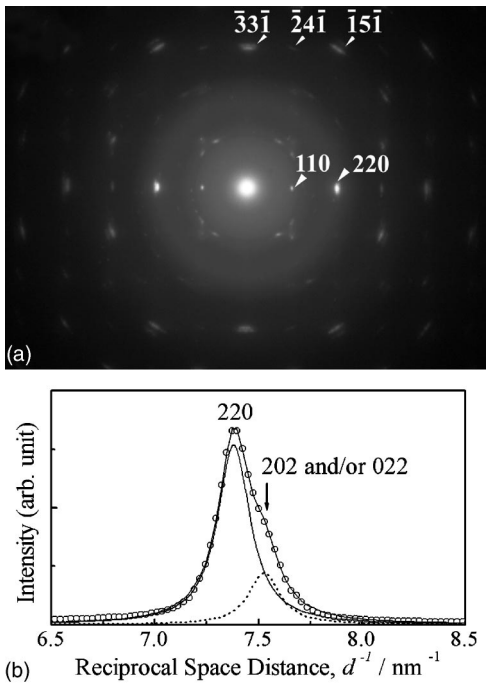

FIG. 5. (a) A SAED pattern with beam incidence of $[\bar{1}\bar{1}6]$. Excitation of the *hh*0 systematic reflections is clearly seen. Here, reflections, 110 and 220, indicated by a single arrowhead come from the $L1_0$−FePd nanoparticles with *c* axes oriented normal to the film plane. (b) A diffracted beam intensity profile measured in the reciprocal space along the $[110]^*$ direction. A shoulder indicates the 202 and/or 022 reflection spots from FePd nanoparticles with *c* axes oriented parallel to the film plane. FePd nanoparticles are well-isolated single crystals with two-dimensional dispersion, so there is no phase relation nor any double diffraction that occurs between these 220 and 202 (or 022) reflections.

Figure 5(a) shows the typical $[\bar{1}\bar{1}6]$ incidence SAED pattern taken at 300 kV for FePd nanoparticles after annealing at 873 K for 3.6 ks. The selected area was about 640 nm in diameter. In the figure, the 110 and 220 reflection spots are indicated by the single arrow heads. An intensity profile measured in the reciprocal space along the $[110]^*$ direction is shown in Fig. 5(b). A subsidiary peak is clearly seen in the profile, indicating a splitting of 220 and 022 (and/or 202) reflection spots, which is due to the existence of three kinds of *c*-axis orientation of the tetragonal nanoparticles in the specimen. Since these 220 and 022 reflections come from different particles with different *c*-axis orientations and also these particles are two dimensionally dispersed on the *a*-Al_2O_3 film, no phase relation exists, nor any double diffraction occurs between these reflections. The 110 and 220 reflections shown in Fig. 5(a) were measured as digital intensity data recorded on IP. Here, the convergent angle of the incident beam was estimated to be 0.19 mrad (semicone angle). The 220 and 202(and/or 022) reflection profiles were separated by means of Lorentzian fitting. A full width at half maximum (FWHM) of the 110 superlattice reflection, 0.21 ± 0.02 nm^{-1}, was also adopted when the FWHM of the 220 intensity was concerned to determine the I_{220} peak height. In the obtained SAED patterns, we selected patterns almost satisfying the condition, $I_{hkl}=I_{\overline{hkl}}$, for order parameter determination. The mean intensity ratio, I_{110}/I_{220}, was 0.199 for the specimen after annealing at 873 K for 3.6 ks.

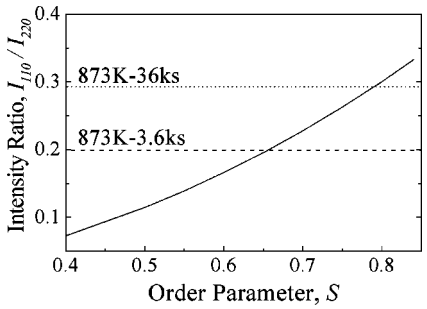

FIG. 6. Order parameter dependence of the intensity ratio I_{110}/I_{220} obtained by the multislice calculations for the 300-kV case (solid curve). The broken and dotted lines indicate the experimentally obtained intensity ratio for specimens after annealing at 873 K for 3.6 and 36 ks, respectively.

In order to evaluate the LRO parameter for the present specimen, we need a relation between the calculated I_{110}/I_{220} ratio and the LRO parameter value. The relation is shown in Fig. 6 on the basis of multislice calculation under the experimental averaged particle thickness of 8.0 nm. The broken line shows the experimentally obtained I_{110}/I_{220} value of 0.199. From Fig. 6, the LRO parameter is determined as 0.65. Using the same method as shown above, we measured the LRO parameter for the specimen after annealing at 873 K for 36 ks. Here, we assumed the averaged specimen thickness as 8.0 nm, since the particle size and its distribution did not change after annealing at 873 K, as shown in Table II. From the intensity ratio I_{110}/I_{220} of 0.293 at 300 kV, we obtained the LRO parameter of 0.79 for the annealed (873 K−36 ks) specimen, as shown in Fig. 6 (dotted line). Considering the mean alloy composition of Fe-58 at. %Pd, the maximum LRO parameter for this alloy is calculated to be 0.84 based on Eq. (1). So the present FePd nanoparticles are judged to be about 90% ordered after annealing at 873 K for 36 ks.

D. Determination of the LRO parameter by high-voltage electron diffraction at 1 MV

A comparison between the intensity ratio I_{110}/I_{220} and the particle thickness relations for fast electrons accelerated at 200, 300 kV, and 1 MV are shown in Fig. 7 under thicknesses below 15 nm. These intensity ratios were calculated under the beam incidence of $[\bar{1}\bar{1}6]$ for $L1_0$-$Fe_{42}Pd_{58}$ ($S=0.8$). The intensity ratio remains almost constant for 1 -MV electrons in the thickness range below 10 nm. Since the

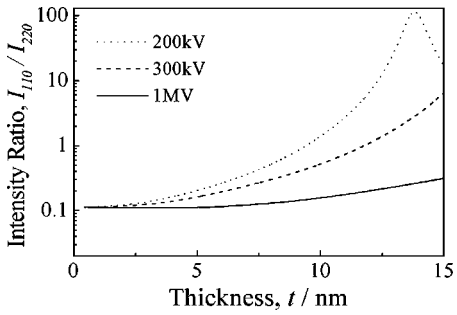

FIG. 7. Thickness dependence of the calculated intensity ratio for three kinds of accelerating voltages. The smallest thickness dependence can be achieved for the 1-MV case.

Downloaded 26 Aug 2011 to 130.34.134.250. Redistribution subject to AIP license or copyright; see http://jap.aip.org/about/rights_and_permissions

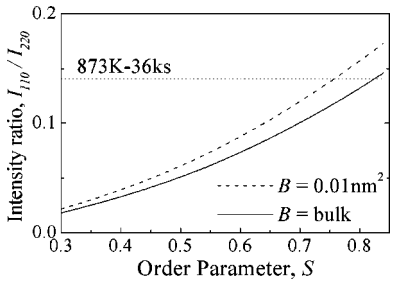

FIG. 8. Order parameter dependence of the intensity ratio I_{110}/I_{220} obtained by the multislice calculations for the 1-MV case. The solid and broken curves are the results obtained under the temperature factors of bulk values and 0.01 nm^2, respectively. The dotted line indicates the experimentally obtained intensity ratio for the specimen after annealing at 873 K for 36 ks.

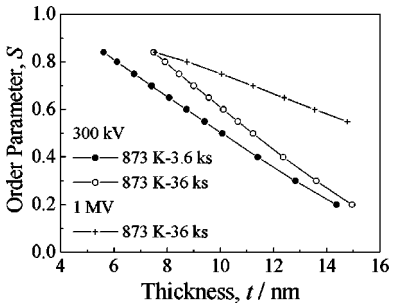

FIG. 9. Apparent thickness dependence of the LRO parameter based on the multislice calculations with experimentally obtained intensity ratios when measured using 300-kV and 1-MV TEMs. It is shown that the LRO parameters decrease apparently with particle thickness in all cases.

intensity ratio is almost independent of the specimen thickness, it is well expected that the experimental error in the thickness estimation less affects the measurement of the LRO parameter under the electron-diffraction experiment at 1 MV. These points will be discussed later. Therefore, it is obvious that the simplified I_{110}/I_{220}-thickness relation at 1 MV is quite useful compared to the cases at 200 or 300 kV. Then we examined the LRO parameter measured from SAED patterns taken at 1 MV. The experimental procedure is the same as mentioned in the previous section. The convergence angle of the electron beam was 0.06 mrad for SAED patterns taken at 1 MV. The mean intensity ratio I_{110}/I_{220} was 0.141 under 1 MV, which gave the LRO parameter of 0.82 as shown by the solid curve in Fig. 8. The obtained LRO parameter is nearly the same as measured by the SAED at 300 kV.

IV. DISCUSSION

In this study we examined the effect of Debye–Waller factor on the accuracy of LRO parameter based on the several reports on the changes of B in the case of nanoparticles. A large increase of B value[22–26] has been reported in Au, Pd, Cu, and Cr nanoparticles, as shown in Table III. For the present FePd nanoparticles with a mean size of 11 nm, the B value is thought to increase compared to bulk FePd alloy to some extent. However, considering the B values listed in Table III, the largest B for the present 11-nm-sized FePd is presumed to be less than 0.01 nm^2. Then we also calculated the intensity ratio under the large B value of 0.01 nm^2 for the 1-MV case and obtained $S=0.76$ for the specimen annealed at 873 K for 36 ks, which is 7.3% smaller than that obtained by the calculation performed under the B values for bulk Fe and Pd. The broken line in Fig. 8 indicates the I_{110}/I_{220}-S relation calculated for the case of $B=0.01$ nm^2. Figure 8 also suggests that the effect of temperature factor on the LRO parameter is enhanced when the degree of order is high. We also examined the effect of the temperature factor on the LRO parameter determined at 300 kV. The LRO parameter decreased to be $S=0.75$ under $B=0.01$ nm^2 for the specimen annealed at 873 K for 36 ks. In respect of the specimen after annealing at 873 K for 3.6 ks, $S=0.62$ was obtained under $B=0.01$ nm^2 at 300 kV, which is 4.6% smaller than that obtained by the calculation performed under the B values for bulk Fe and Pd. In this study we have shown that the temperature factor affects the measured LRO parameter by about 7% at most, though an accurate measurement of temperature factor for FePd nanoparticles as a function of the particle size is desired in the future study. Finally, considering the error of the temperature factor, possible values of the LRO parameters are evaluated as follows under different experimental and specimen conditions:

(i) $S=0.62-0.65$ (300 kV, annealed at 873 K for 3.6 ks),
(ii) $S=0.75-0.79$ (300 kV, annealed at 873 K for 36 ks),
(iii) $S=0.76-0.82$ (1 MV, annealed at 873 K for 36 ks).

Based on the result shown in Fig. 7, it is found that there is a correlation among particle thickness, accelerating voltage, and the LRO parameter. Then we also examined the effect of particle thickness and accelerating voltage on the LRO parameter. We evaluated the LRO parameters under the different thickness using the intensity ratios obtained experimentally. Figure 9 shows the apparent thickness dependence of the LRO parameter under the temperature factors for bulk Fe and Pd. The LRO parameter decreases with the particle thickness in appearance. It should be noted that the amount of decrease in the 1-MV case is smaller than that in the 300-kV case. These thickness dependences of the LRO parameters can be attributed to the accelerating voltage dependence of the diffracted beam intensity ratio shown in Fig. 7; the thickness dependence of the intensity ratio weakens with increasing the accelerating voltage. So the high-voltage TEM has an advantage in determining the LRO parameters, considering the experimental error of the estimated particle thickness compared to the conventional TEMs. It is an essential point that the LRO parameter determined at 300 kV and 1 MV must be the same value for the same specimen,

TABLE III. Debye–Waller factors (B) for several metal nanoparticles at room temperature, where B is defined as $\exp(-2M)=\exp[-2B(\sin\theta/\lambda)^2]$.

	B/nm^2		
Element	Nanoparticle [size/nm]	Bulk	Ref.
Au	0.01 [15]	0.0057	22
Pd	0.0118 [2]	0.0045	23
Cu	0.01 [2]	0.0057	24 and 25
Cr	0.018 [3]	0.0026	26

Downloaded 26 Aug 2011 to 130.34.134.250. Redistribution subject to AIP license or copyright; see http://jap.aip.org/about/rights_and_permissions

when the specimen thickness is determined exactly. From Fig. 9, the LRO parameter of 0.84 is actually obtained as a cross point for the LRO parameter—thickness dependence curves for 300 kV and 1 MV cases when the thickness is 7.6 nm. The thickness value of 7.6 nm is slightly thinner than that estimated by electron holography. In this study, we determined the LRO parameter to be 0.79 and 0.82 using 300-kV and 1-MV TEMs, respectively (annealing: 873 K−36 ks). Slight discrepancy between the LRO parameters determined at 300 kV and 1 MV can be attributed to the experimental error of the estimated particle thickness by electron holography, since we used the theoretical mean inner potential calculated by Eq. (3). However, considering the error of the mean inner potential, presently estimated particle thickness considerably agreed with the thickness evaluated from Fig. 9.

V. CONCLUSION

In the present study, the LRO parameter for 10-nm-sized isolated $L1_0$−FePd nanoparticles with mutual fixed orientation and two-dimensional dispersion has been determined by intensity measurement of electron diffraction with the help of the multislice calculation of electron-diffraction intensities. Excitation of *hh*0 systematic reflections effectively reduces diffracted beams and can largely decrease and simplify the multiple-scattering events among the transmitted and the diffracted waves. Multislice calculations for *hh*0 systematic reflections excited with beam incidences of $[\bar{1}14]$, $[\bar{1}16]$, $[\bar{1}18]$, $[\bar{1}1\ 10]$, and $[\bar{1}1\ 12]$ revealed that the thickness dependence of the intensity ratios I_{110}/I_{220} for these incidences was almost the same. In the present experiments, the *hh*0 systematic reflections were excited using the $[\bar{1}16]$ incidence and the SAED intensities were recorded on IP as digital data. By means of electron-diffraction study at 300 kV, the LRO parameters of 0.65 and 0.79 were obtained for FePd nanoparticles after annealing at 873 K for 3.6 and 36 ks, respectively. The electron diffraction at 1 MV gave the LRO parameter of 0.82 for the specimen annealed at 873 K for 36 ks. A large temperature factor as large as 0.01 nm^2 resulted in a decrease of the LRO parameter by 7.3% at most.

In this article, we have shown the usefulness of a LRO parameter determination by electron diffraction for the ordered alloy nanoparticles epitaxially grown with two-dimensional (2D) dispersion where the usual x-ray diffraction is inapplicable because of the very small volume of the specimen. A combination of electron diffraction under the conditions of *hh*0 systematic reflections and the diffraction experiment at the high accelerating voltage makes the LRO parameter analysis easy and correct. However, evaluation of temperature factors of Fe and Pd atoms in small $L1_0$ nanoparticles is necessary for the more accurate measurement of the LRO parameter.

ACKNOWLEDGMENTS

This study was supported by the Center of Excellence (COE) Program at ISIR-SANKEN, Osaka University, Grant-in-Aid for Scientific Research (Grant Nos. 16106008 and 14205094), Grant-in-Aid for Young Scientists (Grant Nos. 15760490 and 13750612), and Special Coordination Funds for Promoting Science and Technology on "Nanohetero Metallic Materials" from the Ministry of Education, Culture, Sports, Science and Technology, Japan. This study was partly supported by Research Foundation for Materials Science.

[1] E. S. Murdock, IEEE Trans. Magn. **28**, 3078 (1992).
[2] D. N. Lambeth, E. M. T. Velu, G. H. Bellesis, L. L. Lee, and D. E. Laughlin, J. Appl. Phys. **79**, 4496 (1996).
[3] M. H. Kryder, MRS Bull. **21**, 17 (1996).
[4] R. L. White, R. M. H. New, and R. F. W. Pease, IEEE Trans. Magn. **33**, 990 (1997).
[5] D. Weller and M. F. Doerner, Annu. Rev. Mater. Sci. **30**, 611 (2000).
[6] A. Cebollada, D. Weller, J. Sticht, G. R. Harp, R. F. C. Farrow, R. F. Marks, R. Savoy, and J. C. Scott, Phys. Rev. B **50**, 3419 (1994).
[7] M. R. Visokay and R. Sinclair, Appl. Phys. Lett. **66**, 1692 (1995).
[8] B. E. Warren, *X-ray Diffraction* (Dover, New York, 1990), p. 208.
[9] H. Kanazawa, G. Lauhoff, and T. Suzuki, J. Appl. Phys. **87**, 6143 (2000).
[10] S. Okamoto, N. Kikuchi, O. Kitakami, T. Miyazaki, Y. Shimada, and K. Fukamichi, Phys. Rev. B **66**, 024413 (2002).
[11] K. Sato and Y. Hirotsu, Mater. Trans., JIM **44**, 1518 (2003).
[12] P. Hirsch, A. Howie, R. Nicholson, D. W. Pashley, and M. J. Whelan, *Electron Microscopy of Thin Crystals* (Krieger, Florida, 1977).
[13] J. M. Cowley, *Diffraction Physics*, 3rd ed. (Elsevier, Amsterdam, 1995), p. 231.
[14] K. Kaneko, S. Matsumura, K. Ikematsu, Y. Kato, Y. Tomokiyo, M. Watanabe, and T. Masumoto, Scr. Mater. **48**, 915 (2003).
[15] K. Sato and Y. Hirotsu, J. Appl. Phys. **93**, 6291 (2003).
[16] T. Oikawa, D. Shindo, and K. Hiraga, J. Electron Microsc. **43**, 402 (1994).
[17] *International Tables for X-ray Crystallography*, edited by K. Lonsdale (Kynoch, Bermingham, 1962), Vol. III, p. 232.
[18] N. M. Butt, J. Bashir, T. M. Willis, and G. Heger, Acta Crystallogr., Sect. A: Found. Crystallogr. **A44**, 396 (1988).
[19] A. Tonomura, T. Matsuda, T. Kawasaki, J. Endo, and N. Osakabe, Phys. Rev. Lett. **54**, 60 (1985).
[20] J. Endo, T. Matsuda, and A. Tonomura, Jpn. J. Appl. Phys. **18**, 2291 (1979).
[21] D. Rez, P. Rez, and I. Grant, Acta Crystallogr., Sect. A: Found. Crystallogr. **A50**, 481 (1994).
[22] J. Harada and K. Ohshima, Surf. Sci. **106**, 51 (1981).
[23] K. Ohshima, S. Yatsuya, and J. Harada, J. Phys. Soc. Jpn. **50**, 3071 (1981).
[24] M. De Crescenzi, M. Diociaiuti, L. Lozzi, P. Picozzi, and S. Santucci, Phys. Rev. B **35**, 5997 (1987).
[25] F.-W. Telgheder and J. Urban, J. Electron Spectrosc. Relat. Phenom. **95**, 267 (1998).
[26] Y. Kashiwase, I. Nishida, Y. Kainuma, and K. Kimoto, J. Phys. Soc. Jpn. **38**, 899 (1975).

Downloaded 26 Aug 2011 to 130.34.134.250. Redistribution subject to AIP license or copyright; see http://jap.aip.org/about/rights_and_permissions